CEBAF Program Advisory Committee Nine Proposal Cover Sheet

This proposal must be received by close of business on Thursday, December 15 1994 at:

CEBAF
User Liaison Office, Mail Stop 12 B
12000 Jefferson Avenue
Newport News, VA 23606

Proposal Title

PRECISION MEASUREMENT OF THE NEUTRON ASYMMETRY A_1^n AT LARGE X_{Bj} USING CEBAF AT 6 GeV

Contact Person

Name: ZEIN-EDDINE MEZIANI
Institution: TEMPLE UNIVERSITY
Address: DEPARTMENT OF PHYSICS
Address: Barton Hall, 13th & Norris st.
City, State ZIP/Country: Philadelphia, PA 19122 U.S.A.
Phone: (215)204-5971 **FAX:** (215)204-2569
E-Mail → Internet: MEZIANI@VM.TEMPLE.EDU.

Experimental Hall: A **Days Requested for Approval:** 51

Hall B proposals only, list any experiments and days for concurrent running:

CEBAF Use Only

Receipt Date: 12/13/94 PR94-101

By: gp

A proposal for the

PRECISION MEASUREMENT OF THE NEUTRON ASYMMETRY A_1^n AT LARGE x_{Bj} USING CEBAF AT 6 GeV

B. Filippone, W. Korsch, A. Lung, R. Mckeown, M. Pitt
California Institute of Technology, Pasadena, California 91125

J. Gomez, J. Lerose, A. Saha
CEBAF, Newport News, Virginia 23606

P.M. Rutt
University of Georgia and Rutgers University, NJ 08855

B. Anderson, G.G. Petratos, J. Watson
Kent State University, Kent, OH 44242

P. Bogorad, G.D. Cates, K.F. Kumar, H. Middleton
Princeton University, Princeton, NJ 08544

E. Brash, R. Gilman, C. Glashausser, G. Kumbartzki, R.D. Ransome
Rutgers University, Rutgers, NJ 08855

R. Holmes, X. Wang, J. McCracken, P.A. Souder(*co-spokesperson*)
Syracuse University, Syracuse, NY 13122

D. Kawall
Stanford University, Stanford, California 94305

L. Auerbach, Z. Dziembowski, J. Martoff, Z.-E. Meziani(*spokesperson*), J. Park
Temple University, Philadelphia, PA 19122

Abstract

We propose to carry out a world class precision determination of the deep inelastic neutron asymmetry A_1^n in the large x region ($0.25 \leq x \leq 0.63$) and at reasonably high Q^2 ($2.5 \leq Q^2 \leq 5.3$), from a measurement using a high pressure polarized ^{3}He target and the highest available CEBAF energy (6 GeV) polarized beam (see Figure 6 for world data and projection comparison).

The high energy (6 GeV) high current electron beam at CEBAF combined with the good spectrometer resolution of Hall A/C provide a unique opportunity for a precision determination of the photon-neutron spin asymmetry A_1^n in the high x region at large Q^2. The precision attainable at CEBAF will be unchallenged by the high energy facilities around the world engaged in the measurement of this quantity. Previous attempts of this measurement in these facilities lead to a poor statistical uncertainty compared to what can be achieved at CEBAF for reasons summarized below:

- The high duty cycle and high current of CEBAF compensate for the relatively low density ^{3}He polarized target. Therefore the maximum current achievable by the machine is not a limitation.
- For large x, the relatively small incident energy at CEBAF requires a detection of the scattered electron at large angle to reach high x. This in turn provides a large Q^2 but small scattered electron energies due to the large recoil factor. For CEBAF these scattered energies are typically between 1 and 2 GeV leading to a better x resolution compared to any of the high energy spectrometers used around the world.
- The depolarization factor D which is typicaly about 0.3 at any high energy machine can get as large as 0.85 at CEBAF because of the large scattering angle. This is most advantagous when extracting the physics asymmetry A_1^n from the measured asymmetry $A^{\parallel}$.
- A low incident electron energy at CEBAF (6 GeV) compared to those of the high energy machines (20-200 GeV) reduces the decrease of the Mott cross section at large angles for a given x range. This decrease in the cross section is compensated for by the high current available at CEBAF.

A precise determination of the shape of A_1^n in the large x region helps distinguish between the various nucleon models presently under investigation and therefore provide insight into the behavior and interactions of the constituents. This measurement along with the future HERMES high precision measurement of the proton A_1^p and that of the ratio $R^{np} = F_2^n/F_2^p$ in the large x region is of paramount importance for a consistent understanding of the nucleon spin substructure. Moreover, as $x \rightarrow 1$ Perturbative QCD inspired nucleon models offer definite predictions for these quantities and hence can be tested.

We request a total of 51 days which includes a 20% contingency to carry out this precision measurement.

1 Physics Motivation

1.1 Theoretical Motivation

In the last few years there has been a renewed interest in the measurement of the spin structure functions of the nucleon[1,2,4,3,5] because of their direct use in the test of a fundamental QCD sum rule, the Björken sum rule[6]. Another sum rule, which contains specific assumptions on the quark substructure of the nucleon, has also been the focus of an experimental study since its verification/violation gives insight to the nucleon spin structure; this is the Ellis-Jaffe (E-J) sum rule[7].

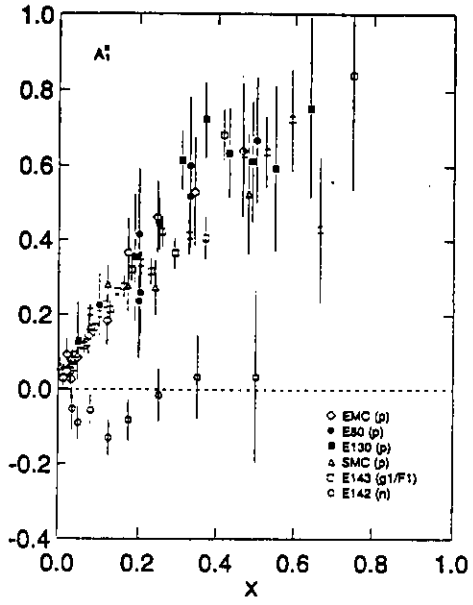

Fig. 1. The World data of $A_1^{n,p}$ on proton and neutron versus x from Ref.[1,2,4,5,3]. Notice the linear scale in x

While the Björken sum rule requires data on the proton and neutron in order to be tested, the E-J sum rule can be examined separately on each of the proton and the neutron. Both sum rules call for the measurement of the asymmetry A_1 over the full range of the Björken variable x within the deep inelastic kinematics. Up to now good statistics on the nucleon's A_1 cover the region $0.003 \leq x \leq 0.5$ for the proton[1,2,4] and $0.05 \leq x \leq 0.3$ for the neutron[5,3] (see Fig. 1).

The present experimental evaluation of the integral $\int_0^1 g_1(x)dx$ displays a systematic uncertainty due to extrapolations of $g_1^n(x)$ in the unmeasured low x and high x regions. The importance of the low x region has been the focus of an intense debate directly related to the possible divergence of the integrand $g_1(x)$ since it is, to first order proportional to $1/x$ in the measured region at low x. Hence, if this behavior extends in the unmeasured region it can impact the verification/violation of the above sum rules. In fact major experimental progams has been launched in several high energy laboratories (CERN, HERA, SLAC) to address the Q^2 dependence of the sum rule (higher twists effects) and the low x extrapolation of $g_1(x)$. These programs concentrate on performing the measurements at the highest average Q^2 and the lowest x possible.

In the debate on the extrapolation procedures for the large x region, it has been argued[16] that the prefered procedure to estimate the uncertainty due to high x extrapolation in most of the existing experiments is to allow $|A_1^n(x)| \leq 1$, rather than by specifying a limiting value." This is because, quoting Ellis and Karliner from Ref.[16]," *models for the polarization asymmetry that combine a non-perturbative Ansatz for the neutron wave function with perturbative QCD at large Q^2 can be used to estimate the limiting value of $A_1^n(x)$ as $x \to 1$, but perturbative QCD alone does not predict a limiting value.* It is therefore important to provide an experimental answer to this unsettled theoretical situation as to the sign of the neutron asymmetry at large at x.

A precision measurement of the photon-nucleon asymmetry A_1 at large x has less impact on the precision of the above sum rules than does the low x measurement, it is nevertheless a rather important measurement for a detailed understanding of the nucleon wave function in terms of its constituents. Moreover as $x \to 1$, Perturbative QCD-guided predictions of the behavior of the ratio

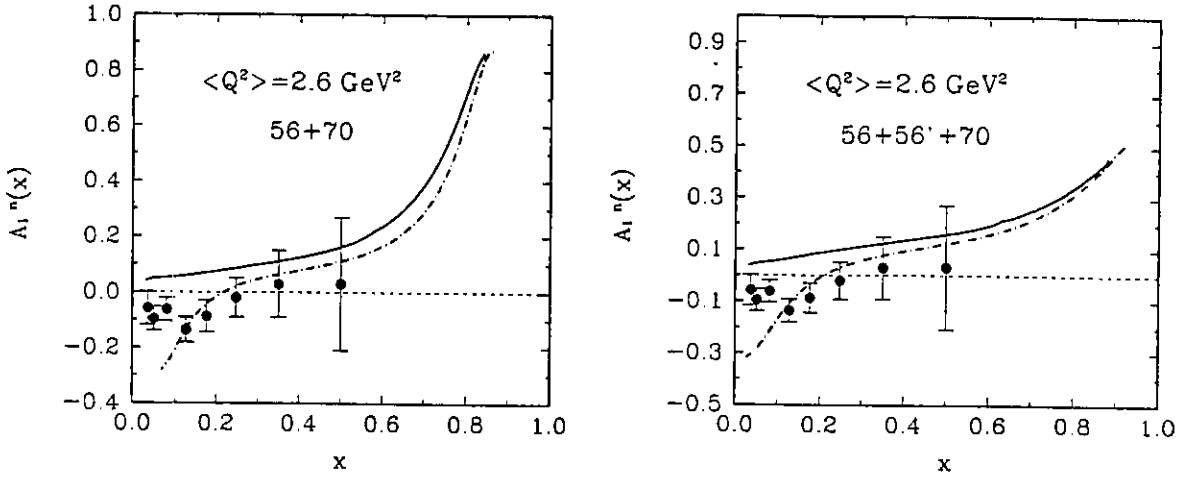

Fig. 2. The neutron spin structure function compared to the data of Ref.[5] curves are from a model described in Ref.[11]. The two full (dashed) solid line is the result (before) after QCD evolution. The right hand side figure includes the 56' component to the nucleon wave function.

of nucleon unpolarized structure functions $R^{n,p} = W_2^n/W_2^p$ and the photon-nucleon asymmetries $A_1^{n,p}$, can be tested.

The behavior of these observables has been discussed extensively in the framework of a three-quark-system nucleon description[8]. If one assumes that among the possible isospin-state diquarks $I = 0$ and $I = 1$ only the $I = 0$ combination survives in the nucleon, then the third quark must carry the isospin of the target. It is a u quark in the proton and a d quark in the neutron, leading to the result $R^{n,p} = 1/4$ and $A^{n,p} = 1$ as $x \to 1$. While no reason is given for the $I = 1$ component suppression, this result is consistent with single flavor dominance, that is the dominance of the u quark in the region $x \to 1$, as the unpolarized data seem to suggest. In this picture the limiting value of $R^{n,p} = 1/4$ also leads to the equality of proton and neutron asymmetries $A_1^p = A_1^n = \frac{u\uparrow - u\downarrow}{u\uparrow - u\downarrow}$ with a limiting value of 1 as $x \to 1$

In 1975 Farrar and Jackson[9] used a colored-quark and vector-gluon model of hadrons to show that a quark carrying nearly all the momentum of the nucleon (i.e. $x \to 1$) must have the same helicity as the nucleon. They procedded to show that quark-gluon interactions cause the $S = 1$, $S_z = 1$ diquark component, rather than the full $S = 1$ diquark system, to be suppressed as $x \to 1$. They obtained the previous limiting value for $A_1^{n,p}$, namely $A_1^{n,p} \to 1$ for $x \to 1$, but found a different bound for the ratio $R^{n,p}$, that is $R^{n,p} = 3/7$ as $x \to 1$. As a reminder we point out that in the naive SU(6) framework where both diquark-spin states $S = 1$ and $S = 0$ contribute equally to the observables of interest, the result is $R^{n,p} = 2/3$ and $A^{n,p} = 1$ as $x \to 1$.

Finally, we want to illustrate the progress achieved in measuring the asymmetry $A_1^{n,p}$ and the ratio $R^{n,p}$ in the valence quark region. We present in Fig. 2 the neutron spin asymmetry A_1^n from the E-142 experiment[5] along with a theoretical evaluation of the nucleon deep inelastic asymmetry within a QCD-inspired quark model[11]. The model is based on a non relativistic constituent quark model with SU(6) symmetry breaking due to a QCD inspired one gluon exchange potential originated by De Rujula, Georgi and Glashow[12] with parameters fixed by Isgur and Karl[13] from the

N-Δ mass splitting. The transformation from the nucleon rest frame to the light cone or infinite momentum frame is performed based on work of Susskind[14], which does not require weak binding or non-relativistic kinematical approximations. QCD evolution is applied to the light-cone distributions to obtain the quark momentum densities. In this model the PQCD limit on A_1 is satisfied for the proton and the neutron. It also predicts the isospin asymmetry manifested by the ratio of unpolarized structure functions $R^{n,p}(x) = F_2^n(x)/F_2^p(x)$ $R^{n,p} = 1/4$, whereas a limiting value of $R^{n,p} = 3/7$ is predicted by Farrar *et. al.*[9] and Ioffe *et.al*[10]. Furthermore, the QCD evolution effects are rather small on $R^{n,p}$, A_1^p and A_1^n, suggesting that the x dependence of $R^{n,p}$, A_1^p and A_1^n in the valence region are essentially low Q^2 effects. Here we point out that the PQCD estimate of Farrar and Jackson[9] includes the SU(6) violation in the photon-quark dynamics, but assumes an SU(6) symmetric structure for the wave function (56 configuration) as $x \rightarrow 1$. Notice the difference in the slope of the asymmetry in the large x region due to the inclusion of the 56' component of the wave function.

On a purely speculative side, most of the available nucleon models give a positive asymmetry in the x region beyond $x = 0.4$. It would therefore be very suprising to observe a negative asymmetry in the large x region, and thus very important to check this possibility experimentally.

While data on $R^{n,p}$ and A_1^p show to some extent indication of the predicted trend for these quantities in the large x region, the experimental situation for the neutron A_1^n is much less clear. The statistical precision of the data at present, does not allow a meaningful statement about the behavior of A_1^n in the large x region. Our motivation is to perform a high precision measurement of the neutron structure function in the large x region which will undoubtedly give insight into the quark substructure of the neutron, but also improve on the precision of the Bjorken and Ellis Jaffe sum rule tests.

1.2 Cross sections and Asymmetries

In deep-inelastic electron scattering, the measured longitudinal asymmetry $A^{\parallel}$ is determined experimentally from measurements of cross sections for polarized electrons on polarized nucleons between states where the helicity are parallel and antiparallel[17,18]:

$$A^{\parallel} = \frac{\sigma^{\uparrow\downarrow} - \sigma^{\uparrow\uparrow}}{\sigma^{\uparrow\downarrow} + \sigma^{\uparrow\uparrow}} = \frac{1-\epsilon}{(1-\epsilon R)\ W_1(Q^2,\nu)}\ [M(E+E'\cos\theta)\ G_1(Q^2,\nu) - Q^2 G_2(Q^2,\nu)] \qquad (1)$$

Here $\sigma^{\uparrow\uparrow}$ ($\sigma^{\downarrow\uparrow}$) is the inclusive $d^2\sigma^{\uparrow\uparrow}/d\Omega d\nu$ ($d^2\sigma^{\downarrow\uparrow}/d\Omega d\nu$) differential scattering cross section for longitudinal target spins parallel (antiparallel) to the incident electron spins. A corresponding relationship exists for scattering of longitudinally polarized electrons off a transversely polarized target where the transverse asymmetry is defined by[18]:

$$A^{\perp} = \frac{\sigma^{\downarrow\leftarrow} - \sigma^{\uparrow\leftarrow}}{\sigma^{\downarrow\leftarrow} + \sigma^{\uparrow\leftarrow}} = \frac{(1-\epsilon)E'}{(1-\epsilon R)\ W_1(Q^2,\nu)}[(MG_1(Q^2,\nu) + 2EG_2(Q^2,\nu))\ \cos\theta] \qquad (2)$$

where R is the ratio of longitudinal-to-transverse virtual-photoabsorption cross sections

$$R = \frac{W_2}{W_1}\ \left(1 + \frac{\nu^2}{Q^2}\right) - 1 \qquad (3)$$

and ϵ is the virtual photon polarization;

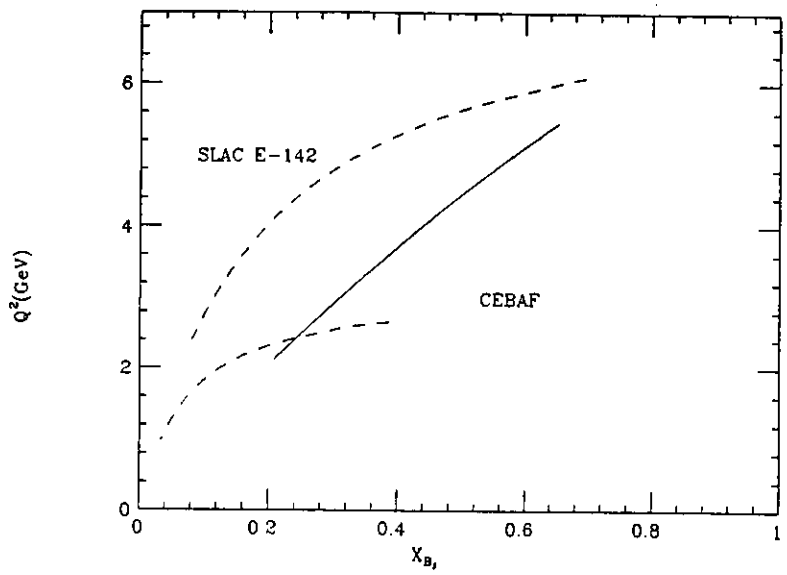

Fig. 3. Kinematic range accessible in this experiment (solid line) compared the the SLAC E-142 kinematics[5] (dashed line). Notice that in this experiment Q^2 larger than 2 $(GeV)^2$ for all x values.

$$\epsilon = \left[1 + 2\left(1 + \frac{\nu^2}{Q^2}\right)\tan^2\frac{\theta}{2}\right]^{-1} \tag{4}$$

Here $\sigma^{\downarrow\leftarrow}(\sigma^{\uparrow\leftarrow})$ is the inclusive scattering cross section for beam-spin antiparallel (parallel) to the beam momentum, and for target-spin direction transverse to the beam momentum and towards the direction of the scattered electron. In all cases, G_1 and G_2 are the spin-dependent structure functions, whereas W_1 and W_2 are the spin-averaged structure functions; M is the mass of the nucleon; Q^2 is the square of the four-momentum of the virtual photon; E is the incident electron energy; E' is the scattered electron energy; $\nu = (E - E')$ is the electron energy loss; and θ is the electron scattering angle.

The system of Eqs. 1 and 2 allows for the separate determination of G_1 and G_2, knowing W_2 and W_1.

The experimental asymmetries $A^{\parallel}$ and $A^{\perp}$ are related to the virtual photon-nucleon longitudinal and transverse asymmetries A_1 and A_2 by the relations

$$A^{\parallel} = D(A_1 + \eta A_2) \tag{5}$$
$$A^{\perp} = d(A_2 - \zeta A_1) \tag{6}$$

where D, d, η and ζ are defined as follows

$$D = (1 - E'\epsilon/E)/(1 + \epsilon R) \tag{7}$$
$$d = D\sqrt{2\epsilon/(1+\epsilon)} \tag{8}$$
$$\eta = \epsilon\sqrt{Q^2}/(E - E'\epsilon) \tag{9}$$
$$\zeta = \eta(1+\epsilon)/2\epsilon \tag{10}$$

- For large x, the small incident energy of the machine requires a detection of the scattered electron at large angle to reach high x. This in turn provides a large Q^2 but small scattered electron energies due to the large recoil factor. For CEBAF these scattered energies are typically between 1 and 2 GeV leading to a better x resolution compared to any of the high energy spectrometers used around the world.

- The depolarization factor D which is typicaly about 0.3 at any high energy machine can get as large as 0.85 at CEBAF because of the large scattering angle. This is most advantagous when extracting the physics asymmetry A_1^n from the measured asymmetry $A^{\parallel}$.

- A low incident electron energy at CEBAF ($6\ GeV$) compared to those of the high energy machines (20-200 GeV) reduces the decrease of the Mott cross section at large angles for a given x range. This decrease in the cross section is compensated for by the high current available at CEBAF.

In table 1 we give a comparison between the relevant parameters at the existing laboratories engaged in the measurement of the nucleon spin structure functions. All kinematics contain a cut $W > 2$ GeV.

Table 1. Comparison of relevant parameters between CERN, HERA, SLAC and CEBAF. Notice the difference in the D factor and size of the x-bin.

Expt. Name	E_i GeV	E' GeV	θ $deg.$	x bin	Q^2 $(GeV/c)^2$	D	P_{e^-,μ^-}	Rate (Hz)
HERMES	35.0	17.0	5.2	0.60-0.70	9.1	0.22	0.50	0.05
SLAC E142	22.66	16.5	7.0	0.40-0.60	5.2	0.27	0.35	7.0
SLAC E143	29.13	25.5	7.0	0.60-0.70	9.1	0.29	0.84	0.3
SMC	190	161	1.8	0.40-0.70	29.5	0.14	0.80	0.005
CEBAF	6.0	1.50	45	0.60-63	5.3	0.85	0.80	0.2

This table shows that the kinematical configuration which would be available at CEBAF with a 6 GeV electron beam energy and the hall A/C spectrometers is unique and would definitely permit the most precise measurement in the high x region.

2 The Experimental procedure

We propose to measure the asymmetry $A_1^{^3He}$ and determine the neutron asymmetry A_1^n with high precision at large x. We shall use the longitudinally polarized ($P_b = 0.8$) high energy CEBAF electron beam ($E_i = 6$ GeV) and a 30-cm-long high pressure double cell polarized ^3He target. The measurement will be performed at one incident electron beam energy ($E_i = 6$ GeV) and one scattering angle ($\theta = 45°$) with ten spectrometer momentum settings covering the range $0.25 \leq x \leq 0.63$ and $Q^2 \geq 2.4$ GeV^2 with $W \geq 2$ GeV. The target polarization orientation can be set longitudinal or tranverse to the beam with a value of $P_t = 0.45$. A beam current of 15 μA combined with a target density of 3.5×10^{21}atoms/cm^2 offers a luminosity of 3.310^{35} cm^{-2}s^{-2} for the proposed measurement. This allows the measurement to be performed in a time period of 1102 hours with beam on target.

The depolarization factor D gives the target polarization projection along the direction of the virtual photon vector $\vec{q}$.

In the scaling limit (ν and Q^2 large), the structure functions in Eqs. 1 and 2 are predicted to depend only on the Bjorken variable $x = Q^2/2M\nu$, yielding

$$MW_1(\nu, Q^2) \rightarrow F_1(x) \quad (11)$$
$$\nu W_2(\nu, Q^2) \rightarrow F_2(x) \quad (12)$$
$$M^2\nu G_1(\nu, Q^2) \rightarrow g_1(x) \quad (13)$$
$$M\nu^2 G_2(\nu, Q^2) \rightarrow g_2(x) \quad (14)$$
$$(15)$$

However, the neutron spin structure function is extracted in the finite Q^2 region following the relation

$$g_1^n(x, Q^2) = \frac{A_1^n F_1^n}{\left(1 + \frac{2Mx}{\nu}\right)} + \frac{A_2^n F_1^n \left(\frac{2Mx}{\nu}\right)^{1/2}}{\left(1 + \frac{2Mx}{\nu}\right)} \quad (16)$$

Within the QPM interpretation, $F_1^n(x)$ and $g_1^n(x)$ are related to the momentum distribution of the constituents as

$$F_1(x) = \frac{1}{2} \sum_{i=1}^{f} e_i^2 \left[q_i^{\uparrow}(x) + q_i^{\downarrow}(x)\right] \quad (17)$$
$$g_1(x) = \frac{1}{2} \sum_{i=1}^{f} e_i^2 \left[q_i^{\uparrow}(x) - q_i^{\downarrow}(x)\right] \quad (18)$$

where i runs over the number of flavors, e_i are the quark fractional charges, and $q_i^{\uparrow}$, $(q^{\downarrow})_i$ are the quark plus antiquark momentum distributions for quark and antiquarks spins parallel (antiparallel) to the nucleon spin.

1.3 Experimental Motivation

From an experimental viewpoint the measurement of the nucleon spin structure function at large x presents challenges when attempted at the high energy machines (CERN, HERA and SLAC). A close examination of all the results or projected results from these experiments shows clearly the statistical limitation of the measurements in the high x region. In fact for the region $x \geq 0.4$ the statistical uncertainty on the neutron measurement is quite large, starting in the best case around $\Delta A_1^n = \pm 10\%$ at $x = 0.4$ and reaching $\Delta A_1^n = \pm 50\%$ at $x = 0.65$. The large scattered lepton energies (greater than 20 GeV) needed to reach high x (0.4-0.7) combined with the spectrometer resolution and the small cross sections give poor results.

A close look at the kinematical parameters suggests that measurements of asymmetry at large x are best performed at CEBAF with incident energies of 6 GeV and greater.

- The high duty cycle and high current of CEBAF compensate for the relatively low density ^{3}He polarized target. Therefore the maximum current achievable by the machine is not a limitation.

2.1 The Polarized Beam

Given the technical developments presently achieved with strained GaAs cathodes at SLAC (E-143) and other places, we hope that high electron beam polarizations (80%) will be as well possible at CEBAF. Although the currents used in experiment E-143 were small (few tens of nanoamps), the next fixed target SLAC experiment in end station A (E-154) is planning to use 80% polarization with few microamps average beam current. SLAC is confident of reaching large electron beam polarizations with high beam currents. I n this proposal we shall assume, that the achievable beam polarization at CEBAF is (80%). To avoid beam depolarization effects on the ^{3}He target we shall limit the beam current to $15\mu A$. We also believe that we can still do a significant measurement even if the polarization of the beam is 50% instead of 80%.

2.2 The Polarized ^{3}He Target

The polarized target will be based on the principle of spin exchange between optically pumped alkali-metal vapor and noble-gas nuclei[21,22,23]. The design will be similar in many ways to that used in E-142, an experiment at SLAC to measure the spin dependent structure function of the neutron. A central feature of the target will be sealed glass target cells, which under operating conditions, will contain a ^{3}He pressure of about 10 atmospheres. As indicated in Fig. 4, the cells will have two chambers, an upper chamber in which the spin exchange takes place, and a lower chamber, through which the eletron beam will pass. In order to maintain the appropriate number density of alkali-metal (which will probably be Rb) the upper chamber will be kept at a temperature of 170–200 ° using an oven constructed of the high temperature plastic Torlon. With a density of 2.5×10^{20} atoms/cm^3, and a lower cell length of 30 cm allowing the end glass windows not to be seen by the spectrometer acceptance. The effective target thickness will be 3.5×10^{21}atoms/cm^2, since the spectrometer acceptance sees a length of 10.cm/sin θ_e= 14.1cm

The target will be in air, or perhaps, in a helium bag. This greatly simplifies the design. The main components of the target are shown in Fig. 4. The main "coils" shown are large Helmoltz coils that will be used to apply a static magnetic field of about 20 Gauss. In addition of establishing the quantization axis for the target, the main coils are important for suppressing relaxation due to inhomogeneities as large as 0.25 G/cm can be tolerated. The NMR components of the target include a set of RF drive coils, and a separate set of pickup coils. Not shown in the figure are the NMR electronics, which will include an RF amplifier, a lock-in amplifier, some bridge circuitry, and the capability to sweep the static magnetic field. The oven shown in Fig. 4 is constructed of Torlon, a high temperature plastic. The oven is heated with forced hot air. The optics system will either include five Ti-Sapphire lasers (only one is shown) or a system of 2-4 laser diodes. Either way,a lens system and a quarter wave plate are required to condition the laser beam and provide circular polarization.

We described some features of the target below in greater detail.

2.2.1 Operating Principles

The time evolution of the ^{3}He polarization can be calculated from a simple analysis of spin-exchange and ^{3}He nuclear relaxation rates[26]. Assuming the ^{3}He polarization $P_{^3He} = 0$ at $t = 0$,

$$P_{^3He}(t) = P_{Rb} \left(\frac{\gamma_{SE}}{\gamma_{SE} + \Gamma_R}\right) \left(1 - e^{-(\gamma_{SE}+\Gamma_R)\,t}\right) \tag{19}$$

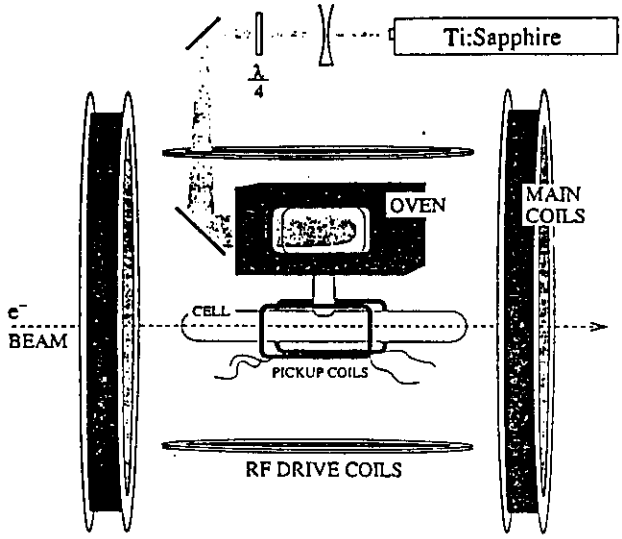

Fig. 4. SLAC E-142 polarized ^{3}He target setup. The CEBAF setup will be similar except that the surrounding medium of the target cell will be air or helium instead of vaccuum.

where γ_{SE} is the spin-exchange rate per ^{3}He atom between the Rb and ^{3}He, Γ_R is the relaxation rate of the ^{3}He nuclear polarization through all channels other than spin exchange with Rb, and P_{Rb} is the average polarization of the Rb atoms. Likewise, if the optical pumping is turned off at $t = 0$ with $P_{^3He} = P_0$, the ^{3}He nuclear polarization will decay according to

$$P_{^3He}(t) = P_0\, e^{-(\gamma_{SE}+\Gamma_R)\,t}. \tag{20}$$

The spin exchange rate γ_{SE} is defined by

$$\gamma_{SE} \equiv \langle \sigma_{SE}\, v \rangle\, [Rb]_A \tag{21}$$

where, $\langle \sigma_{SE}\, v \rangle = 1.2 \times 10^{-19}$ cm^3/sec is the velocity-averaged spin-exchange cross section for Rb–^{3}He collisions[26,30,31] and $[Rb]_A$ is the average Rb number density seen by a ^{3}He atom. The target will be designed to operate with $1/\gamma_{SE} = 8$ hours, a value previously obtained in E142.

From equation (19) it is clear that the best possible ^{3}He polarization is obtained by maximizing γ_{SE} and minimizing Γ_R. But from equation (21) it is also clear that maximizing γ_{SE} means increasing the alkali-metal number density, which in turn means more laser power. The number of photons needed per second must compensate for the spin relaxation of Rb spins. In order to achieve $1/\gamma_{SE} = 8$ hours, about 24 Watts of usable laser light at a wavelength of 795 nm will be required. We will say more about the source of laser light below.

The rate at which polarization is lost, which is characterized by Γ, will have four principle contributions. An average electron beam current of about 15 μA will result in a depolarization rate of $\Gamma_{beam} = 1/30$ hours[37]. Judging from experience at SLAC, we can produce target cells with an intrinsic rate of $\Gamma_{cell} = 1/50$ hours. This has two contributions, relaxation in that occurs during collisions of ^{3}He atoms due to dipole-dipole interactions, and relaxation that is presumably due largely to the interaction of the ^{3}He atoms with the walls. Finally, relaxation due to magnetic field inhomogeneities can probably be held to about $\Gamma_{\nabla B} = 1/100$ hours[35]. Collectively, under operating conditions, we would thus expect

$$\Gamma = \Gamma_{beam} + \Gamma_{cell} + \Gamma_{\nabla B} = 1/30\,\text{hours} + 1/50\,\text{hours} + 1/100\,\text{hours} = 1/16\,\text{hours}.$$

Thus, according to eqn. (19), the target polarization cannot be expected to exceed

$$P_{max} = \frac{\gamma_{SE}}{\gamma_{SE} + \Gamma_R} = 0.66$$

Realistically, a Rb polarization of 100% in the pumping chamber will not be achieved, which will reduce the polarization to about 45–50%.

2.2.2 Target Cells

The construction and filling of the target cells must be accomplished with great care if $1/\Gamma_{cell}$ is to be in excess of 50 hours. We plan to use the "Princeton Prescription" developed for E142. This resulted in lifetimes that were always better than 30hours, and in about 60% of the cells, better than 50 hours. The following precautions will be taken:

- Cells will be constructed from aluminosilicate glass.
- All tubing will be "resized". This is a process in which the diameter of the tubing is enlarged by roughly a factor of two in order to insure that at the resulting glass surface will be pristine, and free of both mechanical defects and chemical impurities.
- Cells will be subjected to a long (4-7 day) bake-out at high (> 400°) temperature on a high vacuum system before filling.
- Rb will be doubly distilled in such a manner as to avoid introducing any contaminants to the system.
- The ^{3}He will be purified either by getters or a liquid ^{4}He trap during filling.

The cells will be filled to a high density of ^{3}He by maintaining the cell at a temperature of about 20 K during the filling process. This is necessary so that the *pressure* in the cell is below one atmosphere when the glass tube through which the cell is filled is sealed.

The length of the cell has been chosen to be 30 cm so that the end windows will not be within the acceptance of the Hall A/C at 45° spectrometers. The end windows themselves will be about 100 μ thick. Thinner windows could in principle be used, but this does not appear to be necessary.

2.2.3 The Optics System

As mentioned above, approximately 20–24 Watts of "usable" light at 795 nm will be required. By "usable", we mean circularly polarized light that can be readily absorbed by the Rb. It should be noted that the absorption line of the Rb has a full width of several hundred GHz at the high pressures of ^{3}He at which we will operate. Furthermore, since we will operate with very high Rb number densities that are optically quite thick, even light that is not well within ther absorption linewidth can still be absorbed.

It is our plan to take advantage of new emerging diode laser technology to economically pump the target. Systems are now commercially available in which a single chip produces about 20 watts of light, about half of which is probably usable. Between 2–4 such systems, at a cost of about

$25,000 each, should do the job. There is also a group a Lawrence Livermore Labs that has offered to build us a single chip that can produce 150 watts. While some studies of the use of diode lasers for spin-exchange optical pumping do exist in the literature[40], actual demonstrations of high polarizations in cells suitable for targets are much more recent[41]. It is our opinion that diode lasers will probably work, and tests will be performed during the E-154 experiment at SLAC.

2.2.4 Polarimetry

Polarimetry will be accomplished by two means. During the experiment, polarization will be monitored using the NMR technique of adiabatic fast passage (AFP)[38]. The signals will be calibrated by comparing the ^{3}He NMR signals with those of water. The calibration will be independently verified by studying the frequency shifts that the polarized ^{3}He nuclei cause on the electron paramagnetic resonance (EPR) lines of Rb atoms[37]. This second technique will be performed in separate target studies, not during the experiment. It will serve solely as a check of our calibration.

2.3 The Spectrometers Setup

We plan to use the Hall A HRS electron spectrometer with its standard detector package which consists of;

- Vertical Drift Chamber's (VDC) for the measurement of momentum and production angle.
- Gas and aerogel Čerenkov counters for pion rejection.
- A set of scintillators hodoscopes for triggering when combined with the Čerenkov counters.
- A lead glass calorimeter for additional pion rejection.

The pion rejection factor with the two Čerenkov counters and the lead glass calorimeter should be better than 10^{-4}. The use of the hadron spectrometer for electron detection is to be considered only for elastic scattering off ^{3}He for calibration and monitoring since its pion rejection factor is only about 10^{-2} when instrumented only with its standard hadron detection package.

Advantages of this measurement advantageous compared to other proposals are;

- The "good" electrons events in the spectrometer are in principle due only to scattering off ^{3}He nuclei. The target cell glass windows are outside the acceptance of the spectrometer
- The excellent target reconstruction by the HRS spectrometers allows for backgrounds originating in the target area to be identified and rejected.
- The excellent resolution of the spectrometer permits the measurement of the product target density by its polarization along the electron beam path using elastic scattering off ^{3}He.

2.4 Proposed Measurements and Data Analysis

The measurement consists of collecting data at one incident energy ($E_i = 6$ GeV) and one scattering angle ($\theta = 45°$) but for six spectrometer momentum settings to cover the range $0.25 \leq x \leq 0.63$.

The raw measured ^{3}He counting asymmetry Δ is converted to the experimental asymmetry $A_{\parallel}^{^3He}$, using the relation

$$A_{\parallel}^{^3He} = \frac{\Delta}{P_b P_t} \tag{22}$$

$$\Delta = \frac{(N^{\uparrow\downarrow} - N^{\uparrow\uparrow})}{(N^{\uparrow\downarrow} + N^{\uparrow\uparrow})} \tag{23}$$

where $N^{\uparrow\downarrow}$ ($N^{\uparrow\uparrow}$) represents the rate of scattered electrons for each bin of x and Q^2 when the electron beam helicity is antiparallel (parallel) to the target spin. $P_b = 0.8$ and $P_t = 0.4$ are the beam and target polarization respectively. The target is long enough (30 cm) so that no dilution of the asymmetry due to its glass windows occurs, however, early in the measurement empty target measurements will be made to insure that no extra dilution of $A_{\parallel}^{^3He}$ occurs from possible background originating in the target area. This study will benefit greatly from the excellent target reconstruction capability of the HRS. The kinematics and electron rates are presented in table 2 where we used a fit of the E-142 data[5] as a model for an estimate of $A_1^{^3He}$ assuming no Q^2 dependence of this asymmetry. The rates where determined using the unpolarized structure functions from the Whitlow 1990 fits[49] to the deep inelastic measurements on proton and deuteron. We added incoherently the appropriate structure functions to generate the ^{3}He cross sections and assumed a luminosity of 3.3 10^{35} cm^{-2}s^{-1}. The times for the longitudinal and transverse measurements where determined by requiring an absolute statistical uncertainty $\Delta A_{\parallel}^{^3He} = 0.0075$ and $\Delta A_{\perp}^{^3He} = 0.015$ and correcting for the target and the beam polarization. The absolute uncertainty $\Delta A_1^{^3He}$ is obtained by propagating the uncertainty from $A_{\parallel}^{^3He}$ and $A_{\perp}^{^3He}$ to $A_1^{^3He}$ using equations (5,6). Fig. 5 (a) shows the projected electron and pion cross sections, where the pion cross sections were generated using the O'Connell and Lightbody code EPCV and (b) the projected results for the ^{3}He asymmetry $A_1^{^3He}$ and for the neutron asymmetry A_1^n.

To evaluate the systematic uncertainty of the corrected asymmetry we assumed $\Delta P_b/P_b = 0.03$ (achievable using a Möller polarimeter) and $\Delta P_t/P_t = 0.05$, which is a reasonable estimate of the relative target polarization uncertainty given our E-142 polarization measurement experience. The total uncertainty in $A_1^{^3He}$ is dominated by the statistical rather than the systematic uncertainty over the full range of measurement.

An elastic scattering asymmetry measurement is planned at small energies (E_i = 1.6 GeV $\theta = 15°$) in order to measure the product of the target density and polarization. This quantity can be evaluated using the measured electric and magnetic form factors of ^{3}He. This measurement would actually determine the polarization of the ^{3}He nuclei along the electron beam path. False asymmetries will be checked to be consistent with zero by comparing data with target spins in opposite directions.

Also contributing to the dilution of the asymmetry is the pair-electron contamination which will be measured by reversing the spectrometer polarity. This correction is x dependent, and is relevant only in the lowest x bins region.

Table 2. Summary of the kinematics and rates of the proposed measurement.

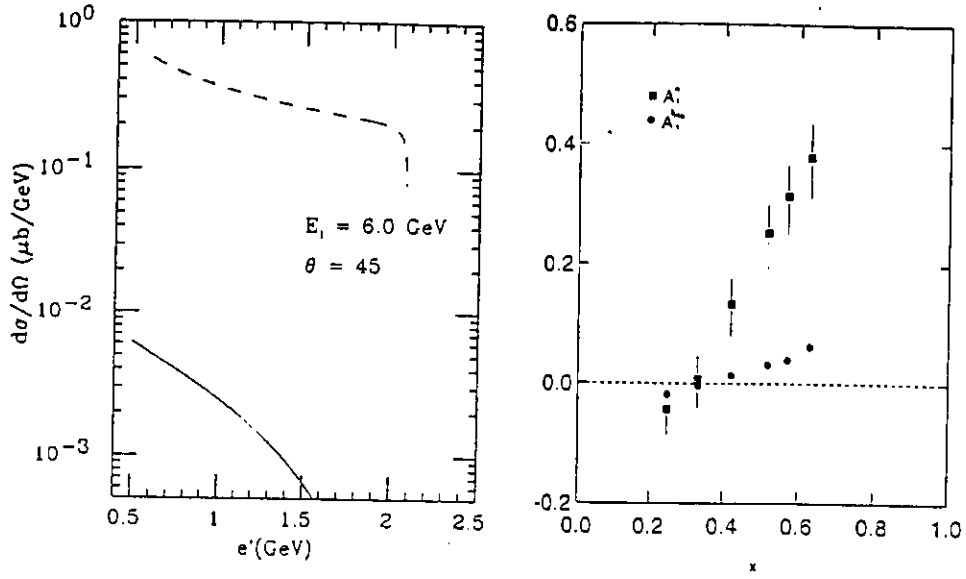

Fig. 5. Projected data for this experiment. Solid circles correspond to the measurement on ^{3}He. The open squares are the projected extracted neutron asymmetry after proton correction. The neutron asymmetry includes statistical and systematic uncertainties added quadratically.

E' (GeV)	x	Q^2 $(GeV)^2$	D	W^2 (GeV)	$A_1^{^3He}$	$\Delta A_1^{^3He}$	$A_2^{^3He}$	$\Delta A_2^{^3He}$	Rate Hz	time$_\parallel$ Hours	time$_\perp$ Hours
1.51	.63	5.3	.85	2.0	0.062	0.0077	0.033	0.0229	0.214	278	44
1.40	.57	4.9	.86	2.1	0.040	0.0075	0.020	0.0232	0.290	205	33
1.30	.52	4.6	.87	2.3	0.031	0.0073	0.014	0.0235	0.363	164	26
1.10	.42	3.9	.90	2.5	0.013	0.0069	0.005	0.0244	0.502	119	19
0.90	.33	3.2	.92	2.7	-0.004	0.0067	-0.001	0.0257	0.614	97	16
0.70	.25	2.5	.95	2.9	-0.018	0.0064	-0.005	0.0279	0.681	87	14

2.4.1 Radiative corrections

The radiative corrections (RC) will be performed in two stages. First the internal corrections will be evaluated following the procedure developed by Bardin and Shumeiko[42] for the unpolarized case and extended to the spin dependent lepto-production cross sections by Akushevish and Shumeiko[43,44]. Second, using these internally corrected cross sections, the external corrections (for thick targets) are applied by extending the procedure developed for the unpolarized cross sections by Tsai[45,46] with modifications appropriate for this experiment. Because of the relatively thin target entrance window ($\sim$ 0.3% radiation length) combined with the exit window thickeness of 1 mm (0.7mm/sin 45° $\sim$ 0.8% r. l.) we expect the external corrections to be small. We point out that all corrections will be carried on the measured parallel $A_\parallel$ and perpendicular $A_\perp$ asymmetries. A_1 is extracted only at the end of the procedure using the required kinematical factors.

The internal corrections will be carried using the program **Polrad version 14** in its iterative method version. In this method the best fit to the experimental asymmetry of ^{3}He is used as a first input to the iterative procedure. The corrected asymmetry is then fitted and used as input to the next iteration step. The process is repeated until convergence is reached, which occurs within four

to five steps.

For reliability **Polrad 14** was checked against a program we developed based on the work by Kuchto and Shumeiko[43] and also against the Tsai[46] formalism for the unpolarized case. Identical results were found with **Polrad 14** with both programs. However the new theoretical treatment used in **Polrad 14** and described in [44] makes "**Polrad 14**" a better tool for performing the RC.

The nuclear coherent elastic tail will be evaluated using different best fits to the elastic form factors of ^{3}He and found to be negligible even at the lowest value of x where its size is the largest. This leaves only three physical regions making significant contributions to the total internal radiative correction; The quasielastic region; the resonance region and the deep inelastic region. The quasielastic region begins few MeV beyond the elastic peak since ^{3}He has no excited states. The beginning of the resonance region is ill somewhat ill defined due to the merging of the quasielastic and resonance tails. The deep inelastic region is assumed to begin at $W = 2$ GeV.

The RC require the knowledge of the spin independent structure functions (SISF) $W_1^{^3He}(Q^2,\nu)$ and $W_2^{^3He}(Q^2,\nu)$ and spin dependent structure functions (SDSF) $G_1^{^3He}(Q^2,\nu)$ and $G_2^{^3He}(Q^2,\nu)$ over the canonical triangle region[46]. The lowest x bin in this measurement ($x = 0.24$) requires the knowledge of the structure functions over the full kinematical range of Q^2 and x. It extends in the range 10 GeV $\leq Q^2 \leq$ 2 GeV and $0.25 \leq x \leq 1$. These variables are converted to the proper integration variables for the RC method defining the canonical triangle given by M_x and t where $M_n + m_\pi \leq M_x \leq W$ and $t_{min} \leq t \leq t_{max}$; $t \equiv Q^2$.

The SISF used in the quasielastic region were those of de Forest and Walecka [47]. These structure functions are not the best available but allow an easy parametrization for a reasonably accurate and fast evaluation of the unpolarized radiative tail. In the resonance region we chose the SISF obtained with careful fitting of data from Ref.[48]. For the deep inelastic region, were previous SLAC measurements where performed, the Withlow global fit[49] was the prefered model for the SISF. Except for the quasielastic region the effect of Fermi motion is only partially included in the evaluation of the deep inelastic structure functions. In other words ^{3}He is considered as made of a deuteron and a proton at rest, so the only spread due to the motion of the nucleons in ^{3}He is represented only by the deuterium width of the quasielastic peak. In the resonance region the SDSF used were obtained from the AO program which is based on an analysis of electromagnetic transition amplitudes in the resonance region[50], while in the deep inelastic region a fit to the extracted $A_1^{^3He}$ from the SLAC experiment[5] E142 was used.

In table 3 we have evaluated the radiative corrections to the asymmetry through five iterations as an estimate of the magnitude of this correction. The correction adds at most $\pm 2\%$ in absolute value to the asymmetry at the highest x bin. The study of systematic effects on the radiative corrections due to model dependence of the SISF and SDSF is still under investigation.

Table 3. Internal Radiative corrections effects using **Polrad 14**. Iteration 5 is the final Born asymmetry while Raw is the measured asymmetry.

E' (GeV)	x	Q^2 $(GeV)^2$	D	W^2 (GeV)	$A_{1r}^{^3He}$ (Raw)	$A_{1c}^{^3He}$ (Iter 1.)	$A_{1c}^{^3He}$ (Iter 3.)	$A_{1c}^{^3He}$ (Iter 5.)	$\Delta A_1^{^3He}$ (Iter. 5-Raw)
1.51	.63	5.3	.85	2.0	0.0619	0.0442	0.0454	0.0402	0.0217
1.40	.57	4.9	.86	2.1	0.0394	0.0291	0.0299	0.0276	0.0118
1.30	.52	4.6	.87	2.3	0.0313	0.0238	0.0243	0.0248	0.0065
1.10	.42	3.9	.90	2.5	0.0135	0.0064	0.0061	0.0116	0.0019
0.90	.33	3.2	.92	2.7	-0.0042	-0.0137	-0.0149	-0.0072	0.0030
0.70	.25	2.5	.95	2.9	-0.0183	-0.0314	-0.0343	-0.0266	0.0083

2.4.2 From ^{3}He to a Neutron

The determination of the inelastic spin-dependent structure function of the neutron from a measurement on ^{3}He relies on our understanding of the reaction mechanism of the virtual photon combined with the use of a realistic ^{3}He wave function. Detailed investigations of the ^{3}He inelastic spin response functions versus that of a free neutron have been carried out by three expert groups in few-body problems[51,52,53]. They examined the effect of the Fermi motion of nucleons and their binding in ^{3}He along with the study of the electromagnetic interaction treatment using the most realistic ^{3}He wave function. Consistent findings have been reached among the three groups, and we summarize here those relevant to our experiment:

- In the deep inelastic region an effective neutron spin structure response can be extracted from that of ^{3}He using a procedure in which S, S' and D states of the ^{3}He wave function are included, but no Fermi motion or binding effects are introduced:

$$\widetilde{g}_1^n = 1/\rho_n(g_1^{^3He} - 2\rho_p g_1^p) \tag{24}$$

$$\widetilde{A}_1^n = \frac{W_1^{^3He}}{W_1^n}\frac{1}{\rho_n}(A_1^{^3He} - 2\frac{W_1^n}{W_1^{^3He}}\rho_p A_n^p) \tag{25}$$

  where $\widetilde{g}_1^n$, g_1^p and $g_1^{^3He}$ are the spin structure functions of an effective free neutron, a free proton and ^{3}He, respectively. Similarly $\widetilde{A}_1^n$, A_1^p and $A_1^{^3He}$ are the photon-target asymmetries for an effective free neutron, a free proton and ^{3}He, respectively. $\rho_n = (87 \pm 2)\%$ and $\rho_p = (-2.7 \pm 0.3)\%$ are the polarization values of the neutron and proton in ^{3}He due to the S, S' and D states of the wave function [52]. *The Convolution approach calculations using the "exact" ^{3}He wave function including the full treatment of Fermi motion and binding effects show negligible differences with the above approximation.* A precise proton measurement is important to minimize the error on the correction. From the presently available proton asymmetry data (SLAC E-80, E-130, E143, CERN EMC and SMC) and that of the neutron (E-142,SMC) we can state that the uncertainty due to nuclear effects is the dominant contribution to the error. At worst, it adds an **absolute uncertainty of $\Delta A_1 \sim 2\%$** to the measured asymmetries at the highest x bin.

- Contrary to the *deep inelastic region* the *quasielastic region* is more sensitive to nuclear effects and has to be treated using the complete convolution method for a reliable extraction of the elastic neutron form factor[53]. We point out that this is **not the case** in this experiment

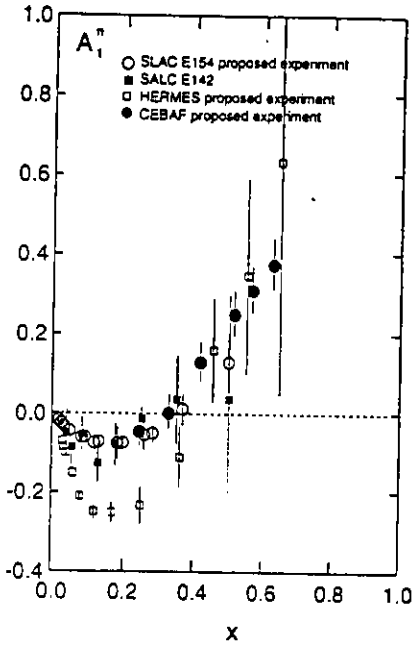

Fig. 6. The World data of A_1^n neutron versus x from Ref.[5,3,56] and world projected data from Ref.[54,55] proposals

since our proposed measurements have a lower limit in missing mass W^2 of 4 GeV^2, already beyond the quasielastic and resonance region.

In summary, in order to extract the neutron asymmetry from the measured ^{3}He asymmetry, we shall follow the method described above[52], allowing for a correction from the polarization of the two protons in ^{3}He ($\sim -2.7\%$ per proton) and a correction for the polarization of the neutron in ^{3}He ($\sim$87%). Starting from the statistical and systematic uncertainties on the measurement of ^{3}He, the neutron asymmetry and its total uncertainty including the above described effects are evaluated and presented in table 4.

Table 4. Uncertainties in the extraction of the neutron asymmetry from the measurement of ^3He.

E' (GeV)	x	Q^2 $(GeV)^2$	W (GeV)	D	$A_1^{^3He}$	$\Delta A_1^{^3He}$ (stat.)	$\Delta A_1^{^3He}$ (syst.)	$\Delta A_1^{^3He}$ (total)	A_1^n	ΔA_1^n (total)
1.51	.63	5.31	2.00	.85	0.062	0.0077	0.0033	0.0084	0.375	0.064
1.40	.57	4.92	2.14	.86	0.039	0.0075	0.0021	0.0078	0.309	0.060
1.30	.52	4.57	2.26	.87	0.031	0.0073	0.0017	0.0075	0.249	0.056
1.10	.42	3.87	2.49	.90	0.014	0.0069	0.0007	0.0070	0.129	0.049
.90	.33	3.16	2.70	.92	-0.004	0.0067	0.0002	0.0067	0.026	0.043
.70	.25	2.46	2.89	.95	-0.018	0.0065	0.0010	0.0065	-0.047	0.039

3 Summary and Beam Request

In summary, We propose to carry out a world class precision determination of the neutron asymmetry A_1^n in the large x region ($0.25 \leq x \leq 0.63$) from a measurement using a high pressure polarized ^{3}He target and the highest available CEBAF energy (6 GeV) polarized beam. (see Figure 6 for world data comparison). This measurement requires 950 hours of beam on target for the measurement of the longitudinal asymmetry and 151 hours for the measurement of the transverse asymmetry, along with 100 hours for spectrometer momentum changes, positron measurements in the lowest three x bins and elastic scattering calibration. We therefore request a total of 1222 hours (51 days) of beam time which includes a 20% contingency on the 1102 hours of beam time on target.

References

[1] M.J. Alguard et al.,, *Phys. Rev. Lett.* **37** (1976) 1258; **37** (1976) 1261.

[2] G, Baum et al., Phys. Rev. Lett. **51** (1983) 1135.

[3] B. Adeva et al., Phys. Lett. B**362** (1993) 352.

[4] J. Ashman et al., Phys. Lett. B**206** (1993) 352; Nucl. Phys. B**328** (1989) 1.

[5] P. Anthony et al., Phys. Rev. Lett. **71** (1993) 959.

[6] J.D. Björken, Phys. Rev. **148** (1966) 1467.

[7] J. Ellis and R.L. Jaffe, Phys. Rev. D**9** (1974)1444; **D10** (1974) 1669.

[8] F. Close, An introduction to Quarks and Partons *Academic Press/ London* 1979.

[9] G. R. Farrar and D. R. Jackson, *Phys. Rev. Lett.* **35** (1975) 1416.

[10] G.R. Farrar *Phys. Letters* **70B** (1977) 346.

[11] Z. Dziembowski, C. J. Martoff and P. Żyla, *Phys. Rev.***D50** (1994) 5613

[12] A. De Rùjula, H. Georgi, and S. L. Glashow, *Phys. Rev.* **D12** (1975)147.

[13] N. Isgur and G. Karl, *Phys. Lett.* **72B** (1977) 109 ;**74B** (1978) 353; *Phys. Rev.* **D19** (1979) 2653; **D20** (1979)1119.

[14] L. Susskind, *Phys. Rev.* **165** (1968) 1535; *Infinite Momentum Frames and Particle Dynamics Vol. 11d, eds. K. Mahanthappa, W. Brittin,* (Gordon and Beach, New York, 1969)

[15] V. A. Khoze and L.N. Lipatov, *Hard Processes Vol.1,* (North Holland Amsterdam, 1984).

[16] J. Ellis and M. Karliner, *Phys. Lett* B**313** (1993)1131.

[17] C.E. Carlson and W.-K. Tung, Phys. Rev. D**5**(1972)721.

[18] A.J.G. Hey and J.E. Mandula, Phys. Rev. D**5**(1972)2610.

[19] L.S. Cardman and C. K. Sinclair, CEBAF memo (1993)

[20] W. Happer, Rev. Mod. Phys. **44** (1972)169.

[21] M.A. Bouchiat, T.R. Carver and C.M. Varnum, Phys. Rev. Lett. **5** (1960)373.

[22] N.D. Bhaskar, W. Happer, and T. McClelland, Phys. Rev. Lett. **49** (1982)25.

[23] W. Happer, E. Miron, S. Schaefer, D. Schreiber, W.A. van Wijngaarden, and X. Zeng, Phys. Rev. A **29** (1984)3092.

[24] R.L. Gamblin and T.R. Carver, Phys. Rev. **138**, A946 (1965).

[25] N.D. Bhaskar, M. Hou, B. Souleman, and W. Happer, Phys. Rev. Lett. **43** (1979)519.

[26] T.E. Chupp, M.E. Wagshul, K.P. Coulter, A.B. McDonald, and W. Happer, Phys. Rev. C **36** (1987)2244.

[27] N.R. Newbury *et al.*, Phys. Rev. Lett. **67** (1991)3219.

[28] B. Larson *et al.* Phys. Rev. Lett. **67** (1991)2901.

[29] A.K. Thompson *et al.*, Phys. Rev. Lett. **68** (1992)2901;

[30] K.P. Coulter, A.B. McDonald, W. Happer, T. E. Chupp, and M.E. Wagshul, Nuc. Inst. Meth. in Phys. Res. **A 270** (1988)90.

[31] N.R. Newbury, A.S. Barton, P. Bogorad, G. D. Cates, M. Gatzke, H. Mabuchi, and B. Saam, Phys. Rev. A **48** (1993)558.

[32] R.J. Knize, Phys. Rev. A **40** (1989)6219.

[33] T.E. Chupp, R.A. Loveman, A.K. Thompson, A.M. Bernstein, and D.R. Tieger, Phys. Rev. C **45** (1992)915.

[34] N. R. Newbury, A. S. Barton, G. D. Cates, W. Happer, and H. Middleton, Phys. Rev. A **48** (1993)4411.

[35] G.D. Cates, S.R. Schaefer and W. Happer, Phys. Rev. A **37**, 2877 (1988); G.D. Cates, D.J. White, Ting-Ray Chien, S.R. Schaefer and W. Happer, Phys. Rev. A **38** (1988)5092.

[36] K.D. Bonin, T.G. Walker, and W. Happer, Phys. Rev. A **37** (1988)3270.

[37] K.P. Coulter, A.B. McDonald, G.D. Cates, W. Happer, T.E. Chupp, Nuc. Inst. Meth. in Phys. Res. A**276** (1989)29 .

[38] A. Abragam, Principles of Nuclear Magnetism (Oxford University Press, New York, 1961).

[39] B. Larson, O. Häusser, P.P.J. Delheij, D.M. Whittal, and D. Thiessen, Phys. Rev. A **44** (1991)3108.

[40] M. E. Wagshul and T. E. Chupp, Phys. Rev. A**40** (1989)4447.

[41] B. Cummings Private communication (1994).

[42] D. Yu. Bardin and N. M. Shumeiko, Nucl. Phys. **B127** (1977)1251.

[43] T.V. Kuchto and N. M. Shumeiko, Nucl. Phys. **B219** (1983)412.

[44] I. V. Akushevich and N. M. Shumeiko, J. Phys. **G**: Nucl. Part. Phys. **20** (1994)513.

[45] L. W. Mo and Y. S. Tsai, Rev. Mod. Phys. **41** (1969)205.

[46] Y. S. Tsai, SLAC-PUB-848 (1971).

[47] T. De Forest and D.J. Walecka Adv. in Phys. 15(1966)57.

[48] F. W. Brasse, W. Flauger, J. Gauler, S. P. Goel, R. Haiden, M. Merkwitz and H. Wriedt, Nucl. Phys. **B110** (1976)413.

[49] L. Whitlow, SLAC-report-357(1990).

[50] S. Kuhn, Private communication and Proposal E-93-009.

[51] B. Blankleider and R.M. Woloshyn, Phys. Rev. C **29** (1984)538.

[52] C. Ciofi degli Atti, S. Scopetta, E. Pace, G. Salme, University of Perugia report N0. DFUPG-75/93 (to be published).

[53] R.-W. Shulze and P.U. Sauer, Phys. Rev. C**48** (1993)38.

[54] HERMES proposal, DESY No. PRC-90-01, R. Milner and K. Rith spokesmen.

[55] SLAC experiment E154, E. Hughes spokesman.

[56] SLAC E143 collaboration experiment; preliminary results.

HAZARD IDENTIFICATION CHECKLIST

CEBAF Proposal No.: _____ Date: _____
(For CEBAF User Liaison Office use only.)

Check all items for which there is an anticipated need.

Cryogenics
- _____ beamline magnets
- _____ analysis magnets
- _____ target
  - type: _____
  - flow rate: _____
  - capacity: _____

Electrical Equipment
- _____ cryo/electrical devices
- _____ capacitor banks
- _____ high voltage
- _____ exposed equipment

Radioactive/Hazardous Materials
List any radioactive or hazadorous toxic materials planned for use:
_____
_____
_____
_____

Pressure Vessels
- 2 cm inside diameter
- 10 atm operating pressure
- Glass window material
- 100 μm window thickness

Flammable Gas or Liquids
- type: _____
- flow rate: _____
- capacity: _____

Drift Chambers
- type: _____
- flow rate: _____
- capacity: _____

Other Target Materials
- ___ Beryllium (Be)
- ___ Lithium (Li)
- ___ Mercury (Hg)
- ___ Lead (Pb)
- ___ Tungsten (W)
- ___ Uranium (U)
- ___ Other (list below)

_____
_____

Vacuum Vessels
- _____ inside diameter
- _____ operating pressure
- _____ window material
- _____ window thickness

Radioactive Sources
- _____ permanent installation
- _____ temporary use
- type: _____
- strength: _____

Large Mech. Structure/System
- _____ lifting devices
- _____ motion controllers
- _____ scaffolding or
- _____ elevated platforms

Lasers
- type: $Argon^{+}$ Ti-Sapphire
- wattage: 20 w
- class: A

Installation:
- _____ permanent
- X temporary

Use:
- _____ calibration
- _____ alignment

Shining on Target cell

Hazardous Materials
- ____ cyanide plating materials
- ____ scintillation oil (from)
- ____ PCBs
- ____ methane
- ____ TMAE
- ____ TEA
- ____ photographic developers
- ____ other (list below)

_____
_____

General:

Experiment Class:

- _____ Base Equipment
- _____ Temp. Mod. to Base Equip.
- _____ Permanent Mod. to Base Equipment
- _____ Major New Apparatus

Other: _____
_____

BEAM REQUIREMENTS LIST

CEBAF Proposal No.: _____ Date: _____
(For CEBAF User Liaison Office use only.)

List all combinations of anticipated targets and beam conditions required to execute the experiment. (This list will form the primary basis for the Radiation Safety Assesment Document (RSAD) calculations that must be performed for each experiment.)

Condition #	Beam Energy (MeV)	Beam Current (μA)	Polarization and Other Special Requirements (e.g., time structure)	Target Material (use multiple rows for complex targets — e.g., w/windows)	Target Material Thickness (mg/cm²)
1	6000	15	80%	Polarized ^{3}He	17.5
				Glass cell Windows	44.6
2	1600	15	80%	^{3}He+Glass	17.5 + 44.6

The beam energies, E_{Beam}, available are: $E_{Beam} = N \times E_{Linac}$ where N = 1, 2, 3, 4, or 5. For 1995, E_{Linac} = 800 MeV, i.e., available E_{Beam} are 800, 1600, 2400, 3200, and 4000 MeV. Starting in 1996, in an evolutionary way (and not necessarily in the order given) the following additional values of E_{Linac} will become available: E_{Linac} = 400, 500, 600, 700, 900, 1000, 1100, and 1200 MeV. The sequence and timing of the available resultant energies, E_{Beam}, will be determined by physics priorities and technical capabilities.

LAB RESOURCES REQUIREMENTS LIST

CEBAF Proposal No.: _____ Date: _____
(For CEBAF User Liaison Office use only.)

List below significant resources — both equipment and human — that you are requesting *from CEBAF* in support of mounting and executing the proposed experiment. Do not include items that will be routinely supplied to all running experiments, such as the base equipment for the hall and technical support for routine operation, installation, and maintenance.

Major Installations *(either your equip. or new equip. requested from CEBAF)*

_____

_____

_____

_____

_____

_____

_____

_____

_____

New Support Structures: _____

_____

_____

Data Acquisition/Reduction

Computing Resources: _____

_____

_____

New Software: _____

_____

_____

Major Equipment

Magnets _____

_____

Power Supplies _____

_____

Targets _____

_____

Detectors _____

_____

Electronics _____

_____

Computer Hardware _____

_____

Other _____

_____

Other

_____

_____

_____

_____

_____